Role of friction in the mechanics of nonbonded fibrous materials

Carine Barbier, Rémy Dendievel, and David Rodney
Science et Ingénierie des Matériaux et Procédés, Institut Polytechnique de Grenoble, CNRS/UJF, 38402 Saint Martin d'Hères, France
(Received 7 May 2009; published 23 July 2009)

Discrete element simulations are employed to study the influence of static friction on the mechanical response of assemblies of nonbonded semiflexible fibers during cycles of isostatic compressions and releases. Hysteresis is evidenced during the cycles and is related to the sensitivity of the frictional contacts on normal forces. Nonzero frictions are shown to decrease both the packing density and caging number but do not affect the critical exponents that characterize the pressure and bulk and shear moduli. Assemblies of frictionless fibers are found fragile in the sense that they resist isostatic compressions but have a zero shear modulus at all densities.

DOI: 10.1103/PhysRevE.80.016115 PACS number(s): 62.20.F−, 81.05.Lg, 87.15.A−

I. INTRODUCTION

Fibrous entangled materials, where the fibers are not permanently linked (i.e., not bonded) have recently attracted much attention because of their relevance in biopolymer mechanics [1]. Their resistance to shear has been quantified since the 1990s for solutions of actin filaments using rheological techniques [2–4], but the study of their resistance to compression dates back to the 1930s and the work of Schofield [5] on animal wools. Since then, very diverse entangled materials have been studied experimentally in compression, including mineral [6], glass [7], and metallic [8] wools (for a study on a wide range of materials, see Ref. [9]). The unique characteristics that emerge from these mechanical studies include: (1) very low volume fractions, (2) deformation by fiber bending between contact points, and (3) highly nonlinear stress-strain relationships in compression.

Linking the overall mechanical behavior of entangled materials to that of their individual fibers remains challenging. Most experimental data are compared to the seminal dimensional analysis of van Wyk [10], which is based on the bending deformation of fibers in a unit cell without slippage at contact points. More refined micromechanical models have been developed for shear and compression, accounting for the distributions of fiber orientations [11], intercontact distances [12,13], and slippage [14,15]. However, all the above models include highly simplifying assumptions, in particular that the segments between contacts are independent from one another and that the motion of the contacts is affine; i.e., it follows the macroscopic (average) strain tensor of the medium. Computer simulations have been used to avoid these assumptions but restricted to bonded systems [6,16–18].

One aspect specific to nonbonded entangled materials is fiber slippage at contact points, which strongly depends on the friction between fibers. Slippage and irreversible fiber rearrangements are evidenced by the hysteresis observed in stress-strain curves during compression-release cycles, both experimentally [8,9,19] and in computer simulations [20,21]. But the influence of friction on such hysteresis is not clear. Also, the effect of friction on compression and shear moduli has been studied so far only for packings of spherical particles [22,23].

We explore the role of friction on the mechanical response to both compression and shear of three-dimensional assemblies of fibers, through discrete element simulations. Our computational model is an extension of that presented in Ref. [24] for frictionless fibers. We study the influence of friction on the hysteresis during compression-release cycles as well as on the packing density, caging number and critical exponents that characterize the fiber networks near the mechanical transition.

II. SIMULATION TECHNIQUE

In the present discrete element method, each fiber is decomposed into N straight segments of same equilibrium length (noted ℓ_0 hereafter). A discretization in segments, rather than in beads as in Ref. [24], reduces the computational time while retaining the accuracy of the calculation if the number of segments per fiber is sufficient (typically four segments per fiber of aspect ratio 20). The behavior of each fiber in traction/compression is modeled by linear springs inside the segments (stiffness K_S). Bending is modeled by angular springs between consecutive segments (stiffness K_B). Despite its simplicity, this model reproduces the main aspects of beam theory [25]: traction, bending, and buckling. First, the fiber Young's modulus is controlled by the linear springs: $E_F=4K_S/(\pi D^2\ell_0)$, where D is the fiber diameter. Second, a fiber of length L clamped at one end and subjected to a transverse force F at the other end deflects by $FL^3/(3\kappa)$ with $\kappa=K_B\ell_0/(1-1/N)/(1-1/2N)\to K_B\ell_0$ when $N=L/\ell_0\to\infty$. Third, a fiber hinged at both ends buckles when subjected to a compressive force exceeding $\frac{K_S}{2\ell_0}(1-\sqrt{1-16\frac{K_B}{K_S}\sin^2(\frac{\pi}{2N})})\to\pi^2\frac{\kappa}{L^2}$ when $N\to\infty$, in agreement with Euler's theory of buckling [25]. The latter result was obtained by considering a straight fiber with segments compressed from ℓ_0 to ℓ. Periodic boundary conditions are employed in order to allow for analytical calculations, but they are applied between 0 and $2L$ in order to allow for bending between 0 and L. If one considers only displacements perpendicular to the fiber axis in a given plane, the nonzero elements of the dynamical matrix in row n (that corresponds to node n) are $D_{n,n}=-2\frac{K_S}{\ell_0\ell}(1-\frac{\ell}{\ell_0})+6\frac{K_B}{\ell^2}$, $D_{n,n+1}=D_{n,n-1}=\frac{K_S}{\ell_0\ell}(1-\frac{\ell}{\ell_0})-4\frac{K_B}{\ell^2}$, and $D_{n,n+2}=D_{n,n-2}=-\frac{K_B}{\ell^2}$. It can be shown by straightforward calculations that this matrix has plane-wave eigenvectors and that the lowest eigenvalue (excluding

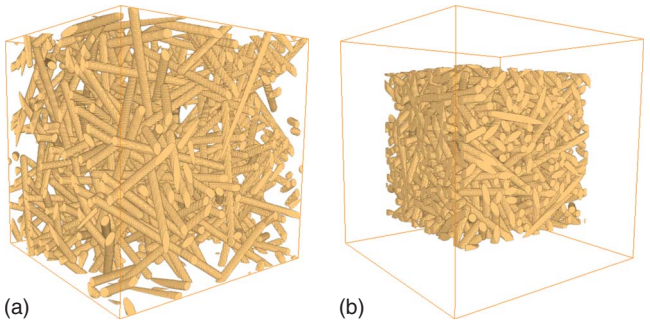

FIG. 1. (Color online) Fiber assembly (a) after an initial relaxation and (b) at the end of a compression phase.

translation) becomes zero for the critical force given above. The associated unstable wave vector is π/L, which corresponds to buckling between 0 and L. We checked by direct computer simulations that the buckling force is not affected by the periodic boundary conditions.

Contact between fibers is modeled through two interaction terms leading to normal and transverse forces at contact points. The first term is a repulsive Hertzian pair potential that acts between two nonconsecutive segments when their distance [26] becomes less than the fiber diameter, leading to normal forces at contact points. The second interaction term models friction between fibers. Each time a new contact is detected, a spring of zero equilibrium length is placed between the two initial contact points on the fiber surfaces. Slippage of the two fibers stretches the spring and produces a transverse force along the fibers. Coulomb's criterion for static friction [27] is applied by removing the spring if the contact is lost or if the norm of the transverse force (i.e., force in the spring at the contact) exceeds the normal force (due to the repulsive potential between fibers) multiplied by a static friction coefficient γ_S. No kinetic friction was implemented, but if at the step following the removal of a spring the fibers are still in contact, the spring is reformed, leading to a stick-slip type of friction. Note that in contrast with studies on spherical particles [22,23], friction is applied here from the outset of the simulations.

We simulated isostatic compressions and releases for assemblies of like fibers initially straight and placed and oriented at random in a cubic cell with periodic boundary conditions. Figure 1 shows two examples of configurations: before and after compression. We considered assemblies of 250 fibers of aspect ratio $(L+D)/D=20$ discretized into four segments in a cell of initial volume $[1.6(L+D)]^3$. The cell volume was decreased (during compressions) or increased (during releases) by increments $\delta V/V=3\%$. This deformation is not applied homogeneously to the fiber nodes because the fibers would be compressed or extended, resulting in an unphysical configuration of high energy since in the equilibrium configurations throughout the simulations, the fibers deform mainly by bending at their contact points and remain nearly at constant length. Thus, between two strain increments, the fibers are rigidly translated with a displacement computed from the affine displacement of their center of gravity. Starting from this configuration, the system is then relaxed using a quenched dynamics algorithm [24]. The compression is carried out until the pressure exceeds a prescribed value ($P=140\ K_B\ell_0/L^4$). The system is then released by increasing the cell volume until no contact remains between fibers and the pressure is less than $10^{-5}\ K_B\ell_0/L^4$. During releases, the fibers are not translated between increments; only the cell volume is increased in order to avoid unphysical separations of the fibers (without inertia, two separating fibers should remain at a distance equal to their diameter). In order not to account for the large nonrecoverable strain produced during the first cycle (as observed experimentally [28]), the system undergoes a first compression-release cycle before the measurements are done. Also, we note that the fiber networks remain isotropic during the compression-release cycles, as evidenced by the fact that the texture tensor $(3\langle \mathbf{n}\otimes\mathbf{n}\rangle$, where the average is taken over the unit vectors, $\mathbf{n}$, of the fiber segments) [29] remains equal to the identity matrix within statistical errors throughout the simulations.

To evaluate the bulk and shear moduli of the assemblies, we start from equilibrium configurations at different densities obtained during the compression of the second cycle and either compress or shear the cell by small increments up to $\pm 1\%$. Simple shear is applied using Lees-Edwards shifted periodic boundary conditions [30]. Note that the shear increments, if applied homogeneously to the fiber nodes, would induce a rotation of the fibers but also spurious compressions or extensions depending on the fiber orientation. The latter is avoided by rotating the fibers and translating them rigidly according to the affine displacement of their center of gravity. The bulk (respectively shear) modulus is then computed from the slope of the pressure (respectively shear stress) as a function of strain.

III. HYSTERESIS DURING COMPRESSION-RELEASE CYCLES

The friction coefficients γ_S considered here range from 0 to 0.8. Figure 2 shows the evolution of the number of contacts per fiber and of the pressure as a function of the relative density of the systems during the second compression-release cycle. We consider first the case without friction ($\gamma_S=0$, black circles in Fig. 2). The mechanical transition already discussed in Ref. [24] is clearly visible in Fig. 2(a). Below the packing density $\rho_C=0.25$, the fibers do not interact. There is no contact between fibers and zero pressure. At ρ_C, the system undergoes a mechanical transition where the number of contacts is discontinuous and reaches a finite value (the caging number, $N_C=8$) while the pressure starts to increase. Upon release, the reverse transition occurs when the number of contacts has returned to eight, confirming that the latter is the minimum number of contacts needed to entangle short fibers. We recall that the caging number decreases for longer and/or more flexible fibers (see Ref. [24]). When the friction coefficient increases from 0 to 0.8, both the packing density and caging number decrease. The reason is that friction stabilizes contacts that otherwise would disappear after fiber slippage such that at a given density the number of contacts increases with friction, and friction makes contacts stronger (they can sustain shear loads) such

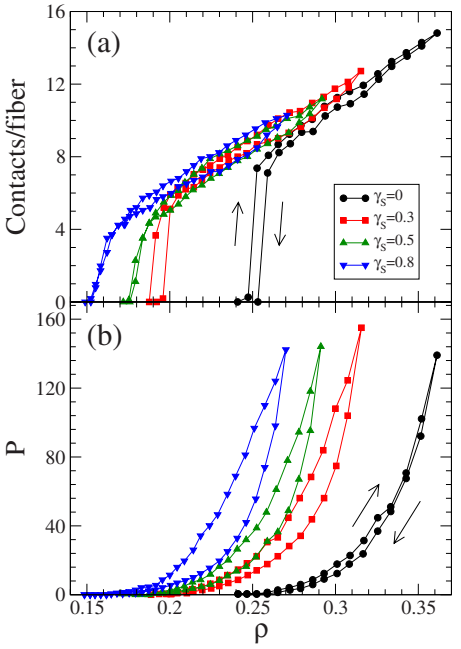

FIG. 2. (Color online) (a) Evolution of the number of contacts per fiber and (b) pressure P as a function of the relative density ρ of fiber assemblies of different static friction coefficients γ_S during a cycle of isostatic compression and release. The arrows show the sense of the cycle. P is normalized by $K_B\ell_0/L^4$.

that less contacts are needed to obtain an entanglement.

Hysteresis is clearly visible in Fig. 2 where, when friction is nonzero, both the number of contacts and pressure decrease more rapidly at the beginning of the release than they increased at the end of the compression. Indeed, the stability of a frictional contact depends on the normal force at the contact through Coulomb's law. Upon unloading, the normal forces decrease, causing a large number of contacts to disappear at the beginning of the release. This reduction in contact number is itself responsible for the rapid decrease in the pressure in Fig. 2(b) and the hysteresis. Without friction, the contacts that form are more stable (because there is nothing to stabilize them other than the fiber entanglement) and they do not depend directly on normal forces. Thus upon unloading, the fiber rearrangements are close to reversible. Note that here no kinetic friction is accounted for and the hysteresis is solely due to irreversible rearrangements of the fibers.

We analyzed the deformation mode of the fibers by comparing their stretching and bending energies, i.e., the energy stored in the linear and angular springs, respectively. Without friction, the stretching energy is negligible and the deformation is mainly accommodated by fiber bending as expected. This remains true at all friction coefficients, but the stretching energy increases with the friction coefficient. The reason is that frictional contacts resist slippage and fibers may thus be stretched between contacts. Interestingly, since the frictional contacts at the origin of the stretching energy are the first to disappear at the beginning of a release phase, the hysteresis on the stretching energy is larger than on the bending energy and increases with the friction coefficient.

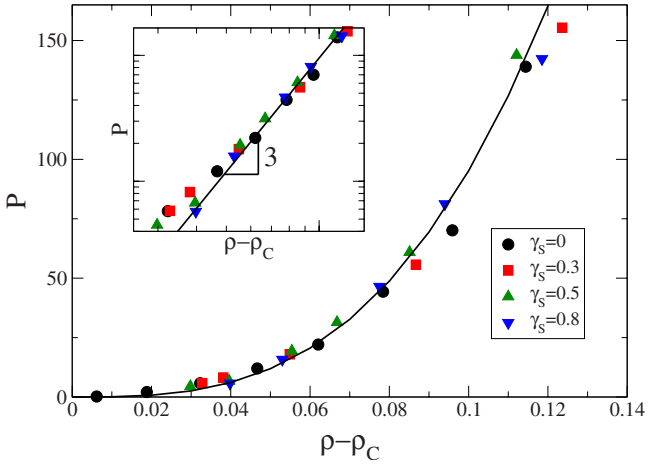

FIG. 3. (Color online) Evolution of the pressure P as a function of the difference between current density ρ and density at transition ρ_C for fiber assemblies with different static friction coefficients γ_S noted on the figure. The solid curve is a power law: $P \propto (\rho-\rho_C)^3$. The inset shows the same data in log scale. P is normalized by $K_B\ell_0/L^4$.

IV. SCALING LAWS

We now turn our attention to the power laws that characterize the evolution of the pressure and of the bulk and shear moduli during the compression of the second cycle. Figure 3 shows the evolution of the pressure, P, as a function of the difference between the current density and the density at transition for different friction coefficients. All data fall on a single curve; i.e., friction affects the packing density but does not change the shape of the pressure curve. The inset in Fig. 3 shows that the pressure follows a power law $P \propto (\rho-\rho_C)^3$, with an exponent $\alpha=3$ in agreement with Van Wyk's analysis [10].

Figure 4 shows the evolution of the bulk modulus, B.

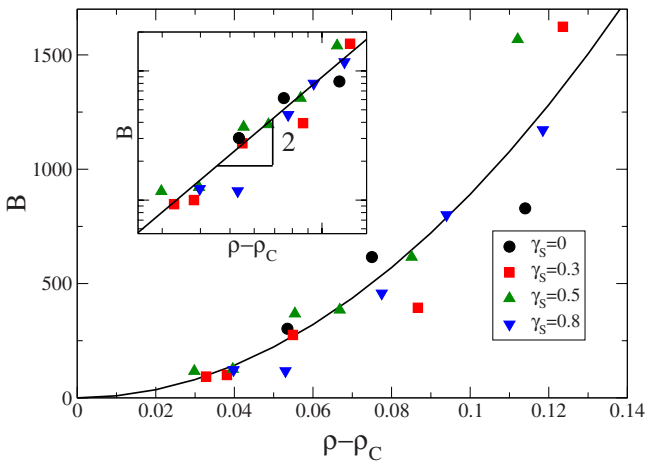

FIG. 4. (Color online) Evolution of the bulk modulus B as a function of the difference between current density ρ and density at transition ρ_C for fiber assemblies with different static friction coefficients γ_S noted on the figure. The solid curve is a power law: $B \propto (\rho-\rho_C)^2$. The inset shows the same data in log scale. B is normalized by $K_B\ell_0/L^4$.

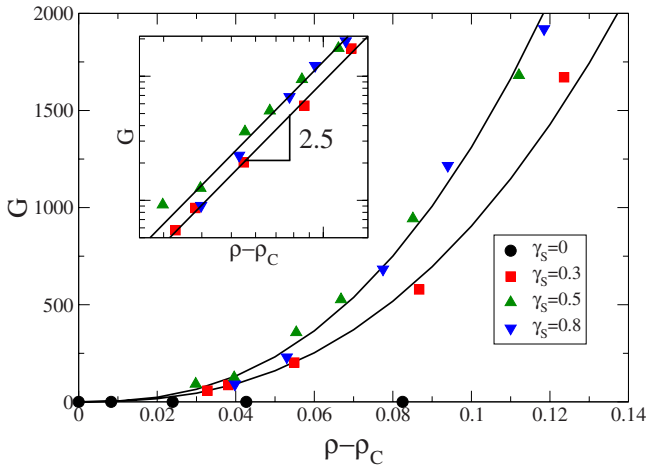

FIG. 5. (Color online) Evolution of the shear modulus G as a function of the difference between current density ρ and density at transition ρ_C for fiber assemblies with different static friction coefficients γ_S noted on the figure. The solid curves are fits: $G \propto (\rho - \rho_C)^{2.5}$. The inset shows the same data in log scale. G is normalized by $K_B \ell_0 / L^4$.

There is more scatter than for the pressure, but the inset shows that the bulk modulus has an exponent $\beta=2$. This exponent is expected from the pressure law discussed above. Indeed, $B=-dP/d\epsilon$ and $\epsilon=\ln(\rho/\rho_C) \sim (\rho-\rho_C)/\rho_C$ close to the transition. Thus, if P has an exponent $\alpha=3$, B has an exponent $\beta=\alpha-1=2$. Note that this relation holds only if the fiber displacement is affine and thus if fiber rearrangements are limited. This is indeed the case for isostatic compressions where the applied strain conserves the symmetry of the environment of the fibers. The latter thus remains close to equilibrium after application of the strain increments and has limited rearrangements during the relaxations. The same conclusion was reached for packing of spheres [22].

Figure 5 shows the evolution of the shear modulus, G. A shear deformation breaks the symmetry of the fiber environments, leading to larger rearrangements than isostatic compressions. Without friction (black circles), the fibers can slide freely with respect to one another and can rearrange upon shear without energy cost. As a result, the shear modulus for frictionless fibers is negligible at all densities. The fibrous system reacts like a fluid with a resistance to isostatic compression but not to shear, illustrating the fragile state of fiber packings, as discussed for spherical particles [31]. Interestingly, G and B are related to Young's modulus E and Poisson's ratio ν in isotropic media (as is the case here) through the relations: $B=E/3(1-2\nu)$ and $G=E/2(1+\nu)$ [25]. Without friction, $B \neq 0$ and $G=0$ imply that $E=0$ and $\nu=1/2$; i.e., the fiber system has no resistance to uniaxial compressions and is incompressible. This can be understood qualitatively: without friction, the fibers can rearrange and flatten perpendicularly to the compression axis, implying a zero Young's modulus, but in doing so, the fibers will press in the orthogonal directions, maintaining the system at constant volume.

When the friction coefficient is not zero, the fiber assemblies resist shear. Figure 5 shows that at all nonzero friction coefficients, the shear modulus has an exponent $\gamma=2.5$, but in contrast with the pressure and bulk modulus, friction affects the prefactor of the power law. The exponent expected from micromechanical models is 3, as for the pressure [13,15]. The difference obtained here is due to nonaffine fiber rearrangements. If we consider the evolution of the shear modulus with friction at a given difference between current and packing densities, the shear modulus increases rapidly between $\gamma_S=0$ and 0.5 and is the same between $\gamma_S=0.5$ and 0.8. Such increase in the shear modulus with friction was reported for spherical particles [22], although the evolution observed here is more rapid.

We note finally that we observed a negative normal stress effect upon shear for nonzero frictions: the stress normal to the shear plane decreases when the system is sheared and the decrease is symmetric for both directions of shear. This effect was first described in the case of cross-linked fibers [32]. A detailed analysis of this effect in the case of nonbonded fibers will be the subject of a future article.

ACKNOWLEDGMENT

The authors would like to thank Professor D. Poquillon for fruitful discussions.

[1] K. Kroy, Curr. Opin. Colloid Interface Sci. **11**, 56 (2006).
[2] F. C. MacKintosh, J. Käs, and P. A. Janmey, Phys. Rev. Lett. **75**, 4425 (1995).
[3] B. Hinner, M. Tempel, E. Sackmann, K. Kroy, and E. Frey, Phys. Rev. Lett. **81**, 2614 (1998).
[4] M. L. Gardel, M. T. Valentine, J. C. Crocker, A. R. Bausch, and D. A. Weitz, Phys. Rev. Lett. **91**, 158302 (2003).
[5] J. Schofield, J. Text. Inst. **29**, T239 (1938).
[6] J. A. Åström, J. Timonen, M. Myllys, J. Fellman, and J. LeBell, Eur. Phys. J. E **22**, 61 (2007).
[7] M. Baudequin, G. Ryschenkow, and S. Roux, Eur. Phys. J. B **12**, 157 (1999).
[8] J. P. Masse, L. Salvo, D. Rodney, Y. Bréchet, and O. Bouaziz, Scr. Mater. **54**, 1379 (2006).
[9] D. Poquillon, B. Viguier, and E. Andrieu, J. Mater. Sci. **40**, 5963 (2005).
[10] C. M. van Wyk, J. Text. Inst. **37**, T285 (1946).
[11] S. Toll, Polym. Eng. Sci. **38**, 1337 (1998).
[12] T. Komori and M. Itoh, Text. Res. J. **61**, 420 (1991).
[13] T. Komori and M. I. Itoh, Text. Res. J. **61**, 588 (1991).
[14] G. A. Carnaby and N. Pan, Text. Res. J. **59**, 275 (1989).
[15] N. Pan and G. A. Carnaby, Text. Res. J. **59**, 285 (1989).
[16] J. Wilhelm and E. Frey, Phys. Rev. Lett. **91**, 108103 (2003).
[17] D. A. Head, A. J. Levine, and F. C. MacKintosh, Phys. Rev. Lett. **91**, 108102 (2003).
[18] E. M. Huisman, T. van Dillen, P. R. Onck, and E. Van der Giessen, Phys. Rev. Lett. **99**, 208103 (2007).
[19] J. I. Dunlop, J. Text. Inst. **65**, 532 (1974).

[20] N. B. Beil and W. W. Roberts, Text. Res. J. **72**, 341 (2002).
[21] N. B. Beil and W. W. Roberts, Text. Res. J. **72**, 375 (2002).
[22] H. A. Makse, N. Gland, D. L. Johnson, and L. M. Schwartz, Phys. Rev. Lett. **83**, 5070 (1999).
[23] H. A. Makse, D. L. Johnson, and L. M. Schwartz, Phys. Rev. Lett. **84**, 4160 (2000).
[24] D. Rodney, M. Fivel, and R. Dendievel, Phys. Rev. Lett. **95**, 108004 (2005).
[25] L. D. Landau and E. M. Lifshitz, *Theory of Elasticity* (Pergamon Press, New York, 1986).
[26] S. Kumar and R. G. Larson, J. Chem. Phys. **114**, 6937 (2001).
[27] E. Rabinowicz, *Friction and Wear of Materials* (Wiley, New York, 1995).
[28] J. I. Dunlop, J. Text. Inst. **74**, 92 (1983).
[29] M. Aubouy, Y. Jiang, J. A. Glazier, and F. Graner, Granular Matter **5**, 67 (2003).
[30] A. W. Lees and S. F. Edwards, J. Phys.: Condens. Matter **5**, 1921 (1972).
[31] M. E. Cates, J. P. Wittmer, J. P. Bouchaud, and P. Claudin, Phys. Rev. Lett. **81**, 1841 (1998).
[32] P. A. Janmey, M. E. McCormick, S. Rammensee, J. L. Leight, P. C. Georges, and F. C. MacKintosh, Nature Mater. **6**, 48 (2007).